ELSEVIER

Thermochimica Acta 384 (2002) 113–120

thermochimica acta

www.elsevier.com/locate/tca

Thermal decomposition of energetic materials 79 Thermal, vibrational, and X-ray structural characterization of metal salts of mono- and di-anionic 5-nitraminotetrazole

B.C. Tappan, C.D. Incarvito, A.L. Rheingold, T.B. Brill*

Department of Chemistry and Biochemistry, University of Delaware, Newark, DE 19716, USA

Abstract

The energetic alkali metal salts (Li^+, Na^+, K^+, Rb^+, Cs^+) of the 5-nitraminotetrazole mono-anion(II) and di-anion(III) were synthesized and their properties compared with neutral 5-nitraminotetrazole(I). The decomposition temperatures by DSC follow the order (III) > (II) > (I), and for the salts of (III) $Li^+ > Na^+ > K^+ > Rb^+ > Cs^+$. Both thermal stability trends are consistent with a major role played by the crystal lattice energy. Loss of H_2O is detected by TGA in cases where hydrates also form. The crystal and molecular structures of Cs(II) and Rb_3(III)$(NCNNO_2)\cdot H_2O$ were determined by X-ray diffraction. The latter compound is the first structural characterization of (III) and also contains the nitrocyanamide anion, $NCNNO_2^-$. The compound $NCNNO_2^-$ appears to have formed by loss of HN_3 from (II) or N_3^- from (III) during one of the synthesis attempts of Rb(II). The major atom motions in the IR spectra of (I), (II), and (III) were assigned on the basis of density functional theory (DFT) using the B3LYP method. Both the IR spectral and crystal structure trends show that increasing the negative charge on the anion primarily shifts the partial double bond character from the C–NNO_2 bond to the CN–NO_2 bond.

Keywords: Thermal decomposition; Structural characterization; 5-Nitraminotetrazole

1. Introduction

Metal salts of 5-nitraminotetrazole(I) have been evaluated for their gas generation [1] and explosive properties [2]. The K^+ [3,4] and Ag^+ [2] salts of the mono-anion(II) have been reported. In addition, all of the Group 1 salts [6] and several transition metal and main group element salts [1,2,7] of the di-anion(III) are known. Of these compounds, the Hg^{2+} salt was identified as having the best potential to be a useful explosive [2]. The structures of (I), (II), and (III) shown here satisfy valence rules but are not intended to represent the true bond orders.

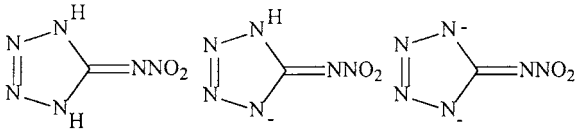

(I) (II) (III)

The exothermic decomposition temperatures of the Group 1 salts of (II) were previously reported [5]; the decomposition mechanisms of the Ag^+ salts have been discussed [7]; and the crystal structures of (I) [8] and the K^+ salt of the 3-methyl derivative of (II) [4] are available. However, a systematic comparative characterization of the chemical properties of these

* Corresponding author. Tel.: +1-302-831-6079; fax: +1-302-831-6335.
E-mail address: brill@udel.edu (T.B. Brill).

0040-6031/02/$ – see front matter
PII: S0040-6031(01)00782-1

materials is not available. To this end, the DSC, TGA, and IR spectral assignments of the Group 1 salts of (II) and (III), along with X-ray crystal structures of the Cs^+ salt of (II) and the Rb^+ double salt of (III) and the nitrocyanamide anion, $NCNNO_2^-$ are reported here.

2. Experimental methods

The Na^+ and K^+ salts of (II) were prepared by the reaction of the metal nitrite and nitraminoguanidine [9]. The Li^+, Rb^+, and Cs^+ salts were made by the reaction of nitroguanyl azide and the metal hydroxide [9]. The Group 1 metal salts of (III) can be made from the reaction of (I) with the metal hydroxide, but cleaner products were obtained by stoichiometric addition of the metal hydroxide to an aqueous solution of the metal salt of (II). The resulting products were dried in a vacuum desiccator, but in several cases they retained H_2O of crystallization. The salts were soluble in H_2O, slightly soluble in DMSO, and, except for the Li^+ salts, are insoluble in organic solvents. The Li^+ salts are somewhat soluble in methanol. Table 1 contains the C, H, and N analyses and stoichiometries.

The transmission IR spectra of the salts were recorded as KBr pellets using a Nicolet 20SXC FTIR spectrometer operating at 4 cm^{-1} resolution. The DSC measurements were made with a DuPont Instruments Model 910 on 0.2–0.5 mg of sample in a sealed Al pan. A heating rate of 10 °C/min was employed. The reproducibility in the exothermic decomposition temperature is about ±5 °C. The TGA measurements were conducted with a DuPont Instruments Model 951 on 3–7 mg of sample with a heating rate of 10 °C/min and a flow of Ar gas.

Many attempts to grow crystals suitable for X-ray diffraction were successful with only the Cs^+ salt of (II), which formed by evaporation of an H_2O solution. In addition, crystals grew from the reaction mixture in which synthesis of the Rb^+ salt of (II) was being attempted. In the latter case, the crystals were actually the one-to-one co-crystallization product of the monohydrated Rb^+ salt of (III) and the Rb^+ salt of nitrocyanamide ($NCNNO_2^-$), i. e. $Rb_3(N_4CNNO_2)$-$(NCNNO_2)\cdot H_2O$. This salt is not the same as the Rb_2(III) salt whose elemental analysis is given in Table 1. Apparently during this singular attempted synthesis of Rb(II), the loss of HN_3 or N_3^- occurred from (II) or (III), respectively. The deazidation process was not investigated further but provided diffraction quality crystals.

Ab initio calculations to optimize the geometries and ground state energies of the anions were performed using the Gaussian 98 package [10] by the B3LYP density functional theory (DFT) method and the 6-31G* basis set. The vibrational spectra were calculated and were multiplied by 0.965, as is customary with DFT to obtain a better match with the observed frequencies. Viewing the modes with the MOLDEN software package [11] provided the major motions that correspond to each frequency. Most of the modes involve strongly internally coupled motions.

3. Properties of the salts

Table 2 gives the exothermic decomposition temperatures for the salts as measured with DSC. In addition small endotherms were observed in the

Table 1
Elemental analyses of Group 1 salts of (II) and (III)

	Calculated (%C)	Observed (%C)	Calculated (%H)	Observed (%H)	Calculated (%N)	Observed (%N)
$Li\cdot H_2O$	7.79	7.95	1.73	2.07	54.55	54.67
$Na\cdot H_2O$	7.06	7.02	1.76	1.75	49.41	47.98
K	7.14	7.18	0.60	1.06	50.00	49.05
Rb	5.59	5.66	0.47	0.59	39.16	38.12
Cs	4.58	4.67	0.38	0.43	32.06	31.41
$Li_2\cdot 2H_2O$	6.74	7.32	2.30	1.87	47.20	44.72
Na_2	7.00	7.45	0.00	0.31	48.28	48.24
K_2	5.83	5.82	0.00	0	40.78	40.01
Rb_2	4.01	3.99	0.00	0	28.09	27.42
Cs_2	3.05	3.10	0.00	0	21.32	21.26

Table 2
Temperatures (°C) of onset of exothermic decomposition

Cation	(II)	(III)
Li	220	411
Na	217	402
K	238	398
Rb	235	391
Cs	212	361

100–110 °C range for the Li^+ salts and one of the Na^+ salts, which was interpreted as resulting from the loss of H_2O of crystallization. The temperature of the exothermic decomposition of the neutral 5-nitraminotetrazole (I) was determined to be 136 °C. With respect to this temperature, the order of stability of the compounds is (III) > (II) > (I). A less definite trend appears to exist in the salts of (III) where the decomposition temperature follows the order $Li^+ > Na^+ > K^+ > Rb^+ > Cs^+$. The former trend correlates with increasing H-atom content and also with increasing lattice energy. The presence of N–H bonds could lower the decomposition temperature by permitting access to decomposition channels that lead to neutral products. That the lattice energy however may be the important factor is suggested by the latter trend in which the cation in the salts of (III) is varied. A decrease in the ionic potential (charge/size ratio) of the cation roughly correlates with a decrease in the decomposition temperature, although the difference is within the reproducibility of the measurement in several cases. A decrease in the lattice energy is expected to occur in the same order. Perhaps, because the difference in the lattice energy is small, the cations have no systematic effect on the decomposition temperatures of the salts of (II).

The energy released upon decomposition of these compounds was difficult to quantify by DSC because the exotherms tended to be very sharp and narrow. The qualitative behavior was indicated however when each was heated slowly on a hot plate. The salts of (II) ignite while those of (III) explode. When subjected to a flame, the salts of (II) burn with flashes, while the salts of (III) give a muffled pop.

TGA of the Li^+ and Na^+ salts of (II) and (III) and showed a gradual but distinct loss of weight in the 100–150 °C range, which is undoubtedly the result of loss of H_2O of crystallization. The Na^+ salt of (II) lost 10.9% of the sample weight, which corresponds to one H_2O per formula unit. The Li^+ salts of (II) and (III) showed a 22.00 and 20.23% weight loss respectively, corresponding to two H_2O molecules per formula unit. The Li^+ salt also forms a monohydrate whose elemental analysis was obtained (Table 1).

TGA and DSC were performed on $Rb_3(N_4CNNO_2)(NCNNO_2)\cdot H_2O$ for which suitable crystals were obtained for X-ray crystallography. A loss of 3.2% of the sample weight occurred in the range of 60–100 °C, which is in fair agreement with the loss of one H_2O per formula unit (3.7%). The endotherm for this event in the DSC occurs at about 120 °C, and is at a higher temperature than the TGA value possibly because of the restriction of evaporation by the crimped pan. Distinct exotherms appear at 300 and 383 °C corresponding to the decomposition of the nitrocyanamide ion and the nitraminotetrazole dianion, respectively.

4. X-ray crystallography

The crystal structure of the neutral (I) co-crystallized with a molecule of H_2O and half a molecule of dioxane in the asymmetric unit was previously known from work in this laboratory [8]. In the present work, the Cs^+ salt of (II) grew large single crystals by the slow evaporation of a water solution. The crystals adopted the monoclinic space group $P2_1/c$, with four molecules in the unit cell. Table 3 lists the crystal, data collection, and refinement parameters. Table 4 lists the atomic coordinates and Table 5 gives the bond distances and bond angles. Fig. 1 shows the structure of the planar ion (II) and the relative positions of the Cs^+ ions. The projection shown illustrates the intermolecular interactions.

Because of the high electron density of the Cs^+ ions, the electron density corresponding to the H-atom attached to (II) could not be refined with a high degree of certainty. However, a region of higher electron density is located about 0.9 Å from N(4). The residual electron density near N(1), the other likely H-atom location, was about one-third less than that near N(4)). Thus the H-atom is probably attached to N(4). For comparison, the two hydrogen atoms of (I) were located on N(1) and N(4) on the basis of hydrogen bonding [8].

Table 3
Crystal parameters and data collection for the Cs^+ salt of (II) and Rb^+ double salt of (III) and the nitrocyanamide anion

(a) Crystal parameters		
Formula	$CHCsN_6O_2$	$C_2H_2N_9O_5Rb_3$
Space group	$P2_1/c$	$C2/c$
Crystal system	Monoclinic	Monoclinic
a (Å)	5.145 (18)	23.244 (9)
b (Å)	17.982 (9)	7.077(3)
c(Å)	6.433 (4)	14.810 (7)
β (°)	92.46(4)	91.35 (3)
V (Å^3)	594.7(5)	2435.4(17)
Z	4	8
Crystal dimensions (mm^3)	0.3 × 0.3 × 0.3	0.3 × 0.4 × 0.4
Crystal color	Colorless	Colorless
Density (calculated, g/cm^3)	2.926	2.605
Temperature (K)	244(2)	250(2)
(b) Data collection		
Diffractometer	Siemens P-4	Siemens P-4
Monochromator	Graphite	Graphite
Scan technique	Omega Phi	Omega phi
Independent reflections	990 (R_{int} = 0.0528)	1759 (R_{int} = 0.0850)
Θ Scan range (°)	2.27–25.02	2.75–23.99
Completed at	94.3% (Θ = 25.02°)	92.4% (Θ = 23.99°)
(c) Refinement		
Refinement method	Full-matrix least-squares on F^2	
Final R indices	$R1$ = 0.0252 (w$R2$ = 0.0746)	$R1$ = 0.0773 (w$R2$ = 0.1904)
R indices (all data)	$R1$ = 0.0267 (w$R2$ = 0.0753)	$R1$ = 0.1061 (w$R2$ = 0.2071)
Largest diffraction peak/hole (eÅ^{-3})	0.844 and −0.411	1.646 and −1.712
GOF	1.495	1.336

The crystal structure of $Rb_3(N_4CNNO_2)(NCNNO_2)\cdot H_2O$ was a surprise in that not only was the structure of (III) obtained for the first time, but it was found to be the double salt the $NCNNO_2^-$ ion whose structure was recently reported [12]. Fig. 2 shows the structural units in their relative locations in the crystal lattice, while Table 6 gives the atomic coordinates and Table 7 gives selected bond distances and angles. Both (III) and the nitrocyanamide anion are planar molecules.

Table 4
Atomic coordinates (× 10^4) and isotropic thermal parameters (Å^2 × 10^3) for Cs^+(II)[a]

	x	y	z	U (eq)
Cs(1)	5601.0(5)	6745.3(3)	1402.1(5)	27(1)
O(1)	10404(6)	7459(2)	4693(5)	31(1)
O(2)	12969(6)	6619(2)	6068(6)	29(1)
N(1)	6905(6)	5367(2)	7280(5)	21(1)
N(2)	7874(7)	4696(2)	7884(6)	25(1)
N(3)	10385(7)	4680(2)	7823(5)	23(1)
N(4)	11127(6)	5361(2)	7174(5)	19(1)
N(5)	8607(6)	6477(2)	6026(6)	21(1)
N(6)	10734(7)	6848(2)	5623(6)	20(1)
C(1)	8971(7)	5777(2)	6818(6)	16(1)

[a] U (eq) is defined as one-third of the trace of the orthogonalized U^{ij} tensor.

Table 5
Bond lengths (Å) and angles (°) for Cs^+(II)

Bond lengths (Å)		Bond angles (°)	
O(1)–N(6)	1.260(4)	O(2)–N(6)–O(1)	120.2(3)
O(2)–N(6)	1.243(5)	O(2)–N(6)–N(5)	123.7(3)
N(1)–C(1)	1.338(5)	O(1)–N(6)–N(5)	116.0(3)
N(1)–N(2)	1.356(5)	N(3)–N(2)–N(1)	111.4(3)
N(2)–N(3)	1.295(5)	C(1)–N(4)–N(3)	108.3(3)
N(3)–N(4)	1.354(5)	N(2)–N(3)–N(4)	106.5(3)
N(4)–C(1)	1.349(5)	N(1)–C(1)–N(4)	108.1(3)
N(5)–N(6)	1.317(5)	N(1)–C(1)–N(5)	119.5(3)
N(5)–C(1)	1.368(5)	N(4)–C(1)–N(5)	132.2(3)
		N(6)–N(5)–C(1)	115.9(3)
		C(1)–N(1)–N(2)	105.6(3)

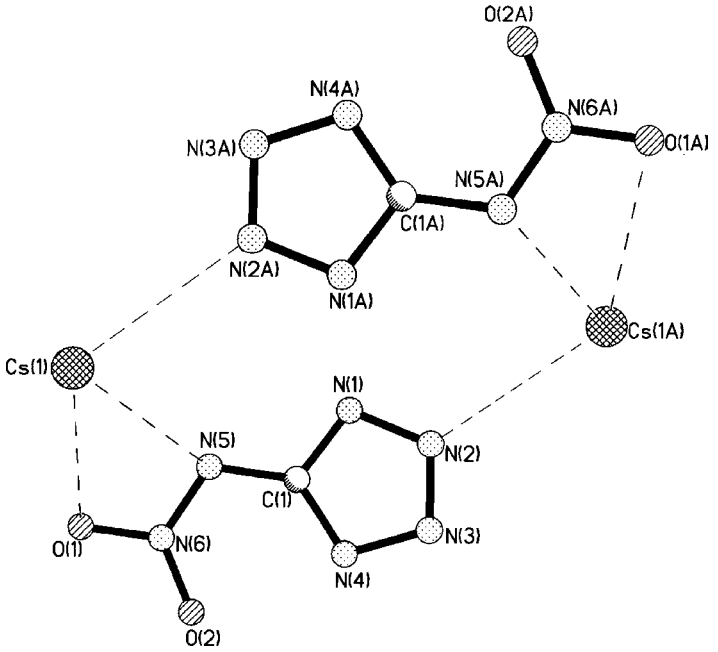

Fig. 1. The molecular structure of Cs(II) showing the relative positions of the rings and Cs atoms in the lattice.

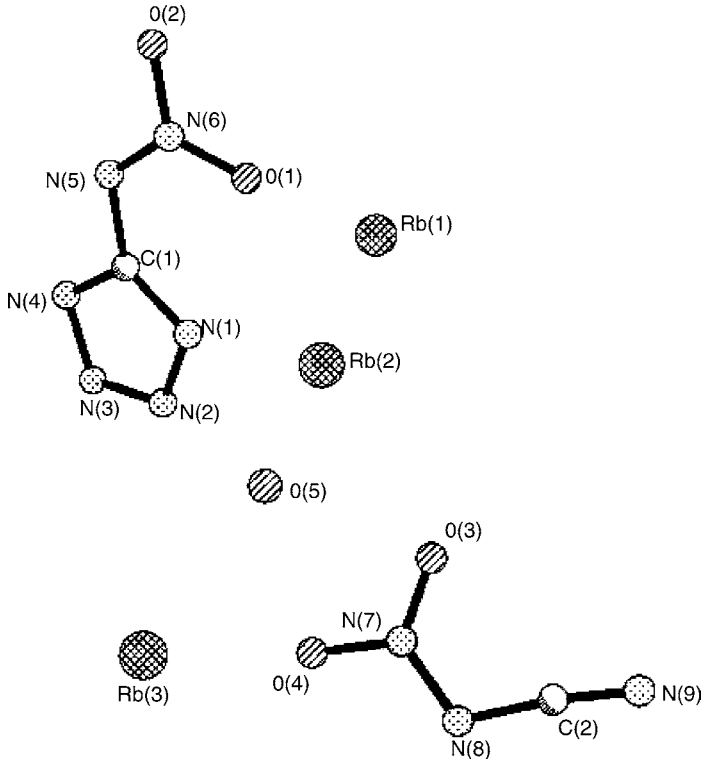

Fig. 2. The molecular structures of (III) and the nitrocyanamide anion and the relative positions of the ions in the crystal lattice of Rb_3(III)(nitrocyanamide)·H_2O.

Table 6
Atomic coordinates ($\times 10^4$) and equivalent isotropic displacement parameters ($\mathring{A}^2 \times 10^3$) for $Rb_3(N_4CNNO_2)(NCNNO_2)\cdot H_2O$[a]

	x	y	z	U (eq)
Rb(1)	−1506(1)	−914(2)	2833(1)	17(1)
Rb(2)	−2983(1)	−1165(2)	3863(1)	16(1)
Rb(3)	−4679(1)	2053(2)	4184(1)	21(1)
O(1)	−1877(4)	−580(15)	4764(7)	19(2)
O(2)	−1286(4)	−2(15)	5916(6)	14(2)
O(3)	−3942(6)	−1890(20)	2570(9)	41(3)
O(4)	−4246(6)	950(20)	2457(9)	46(4)
O(5)	−4236(5)	−1583(15)	4887(7)	21(3)
N(1)	−2219(6)	2413(19)	3708(9)	18(3)
N(2)	−2363(6)	3865(18)	3180(9)	18(3)
N(3)	−2092(6)	5380(20)	3436(9)	24(3)
N(4)	−1759(5)	4969(18)	4175(8)	13(3)
N(5)	−1538(5)	2396(17)	5064(8)	10(3)
N(6)	−1586(5)	610(17)	5235(8)	12(3)
N(7)	−4256(5)	−740(19)	2202(9)	19(3)
N(8)	−4643(6)	−1190(20)	1604(9)	24(3)
N(9)	−4627(8)	−4510(30)	1155(12)	53(5)
C(1)	−1840(6)	3140(20)	4312(10)	8(3)
C(2)	−4617(7)	−3020(30)	1408(12)	27(4)

[a] U (eq) is defined as one-third of the trace of the orthogonalized U^{ij} tensor.

A comparison of the structures of (I), (II), and (III) reveals that almost all of the bond lengths and angles are within three times the error in the determination. Most of the differences are therefore indistinguishable.

Table 7
Bond lengths (Å) and angles (°) for Rb_3(III)(nitrocyanamide)

Bond lengths (Å)		Bond angles (°)	
(III)			
O(1)–N(6)	1.277(15)	N(2)–N(1)–C(1)	104.4(12)
O(2)–N(6)	1.288(14)	N(3)–N(2)–N(1)	110.7(12)
N(1)–N(2)	1.329(18)	N(2)–N(3)–N(4)	108.6(13)
N(1)–C(1)	1.342(18)	C(1)–N(4)–N(3)	104.8(12)
N(2)–N(3)	1.299(19)	N(6)–N(5)–C(1)	118.4(11)
N(3)–N(4)	1.356(17)	O(1)–N(6)–N(5)	125.8(11)
N(4)–C(1)	1.324(19)	O(2)–N(6)–N(5)	115.6(11)
N(5)–N(6)	1.295(17)	N(1)–C(1)–N(5)	133.8(13)
N(5)–C(1)	1.406(17)	N(4)–C(1)–N(1)	111.4(12)
		N(4)–C(1)–N(5)	114.7(12)
Nitrocyanamide			
O(4)–N(7)	1.253(19)	O(4)–N(7)–N(8)	116.7(14)
O(3)–N(7)	1.212(17)	N(7)–N(8)–C(2)	110.8(14)
N(7)–N(8)	1.287(18)	O(3)–N(7)–N(8)	123.2(15)
N(8)–C(2)	1.33(2)	O(3)–N(7)–O(4)	119.8(14)
N(9)–C(2)	1.12(2)	N(9)–C(2)–N(8)	172.0(2)

Table 8
Bond lengths (Å) in the $CNNO_2$ unit of 5-nitraminotetrazole as a function of the charge

Bond	(I)	(II)	(III)
C–NNO_2	1.344	1.368	1.406
N–NO_2	1.331	1.317	1.295
N–O	1.245	1.252	1.282

The bond distances generally are much shorter than the single bond distances (C−N = 1.475 Å, N−N = 1.45 Å, and N−O = 1.40 Å), which reflects the high degree of p-electron delocalization throughout these molecules. The N(2)–N(3) distance of 1.295 Å shows the highest degree of multiple bond character. Despite the similarity of the structures of the anions, the different charges cause a notable redistribution of electron density in the $CNNO_2$ substituent. Table 8 compares the bond distances in the C–N–NO_2 unit as a function of the charge. As the negative charge increases, the N–N bond shortens while the C–N and N–O bonds lengthen. By electrostatic repulsion the increased negative charge on the ring in effect forces the partial double bond character in the C–N–NO_2 unit to redistribute to some extent out of the C–N bond and into the N–N bond.

5. Vibrational motions

The mid-IR spectra of the salts of (II) and (III) in this study were recorded and found to depend very little on the counter cation. The spectra of (I), (II) and (III) display several significant differences, and the assignment of most of the modes is complicated by the substantial coupling of the like-atom motions in the conjugated structure. To resolve this problem the motions corresponding to the absorptions were identified by calculation of the energies using DFT and observation of the motions using the MOLDEN package. No cation was included in the calculation.

Tables 9–11 list the calculated and observed frequencies for (I), (II), and (III) in the finger print region, along with the qualitative description of the atoms or groups that dominate the motion in each case. This information on assignments is useful because some of the frequency differences can be understood on the basis of the charge-dependent electron density

Table 9
Calculated and observed vibrational modes (per centimeter) and major atom motions for (I)[a]

Calculated	Observed	Description
1677	1680w	C–N stretch
1607	1613vs	NO_2 asymmetric stretch
1496	1508vs	N(3)–N(4) stretch + C–NNO_2 stretch
1396	1406w	N–C–N asym stretch
1375	1397w	N–C–N asym stretch
1335	1315vs	N–NO_2 asym stretch with N–H wag
1233	1226s	N–NO2 and C–N stretch
1084	1054m	N–C–N sym stretch
1022	1021m	N–N ring asym stretch
987	995m	N–NO_2 stretch
841	878w	C–N–NO_2 bend
775	781m	N–N(O)O out of plane oscillation
751	752vw	C–N–NO_2 bend
725	714m	N–H wag
713	714m	C out of plane oscillation
614	652w	N–H out of plane bend

[a] vs = 90−100%, s = 70−90%, m = 40−70%, w < 30%.

redistribution uncovered above in the crystal structure data (Table 8). The predominately C–NNO_2 stretch decreases in energy (i.e. the bond lengthens) as the negative charge on the ion increases [1680 cm^{-1} (I), 1545 cm^{-1} (II), 1452 cm^{-1} (III)]. At the same time,

Table 10
Calculated and observed vibrational modes (per centimeter) and major atom motions for (II)[a]

Calculated	Observed	Description
1557	1546s	C–N5 stretch
1469	1423vs	NO_2 asymmetric stretch
1365	1355vs	Coupled NO_2 and N1–C–N4 symmetric stretch
1332	1342vs	N–H wag, ring stretch
1306	1315vs	N–NO_2 stretch coupled with N2–N3 stretch
1208	1225s	C–N–NO_2 asym stretch, N3–N4 asym stretch
1148	1147m	N–NO_2 and N3–N4 stretch with N–H wag
1094	1096m	Ring breathing
1037	1031m	N–H wag with sym NNO_2 breathing
1021	1061s	N3–N4 stretch
1003	999m	N3–N4 stretch
854	864w	C–N–NO_2 bend
774	775w	N–NO_2 out-of plane oscillation
751	747w	NO_2 scissor with C–N–NO_2 bend
613	697w	Hydrogen out of plane wag

[a] vs = 90−100%, s = 70−90%, m = 40−70%, w < 30%.

Table 11
Calculated and observed vibrational modes (per centimeter) and major atom motions for (III)[a]

Calculated	Observed	Description
1444	1452s	C–N5 stretch
1379	1398vs	N–NO_2 stretching
1323	1295s	NO_2 asym stretch
1125	1145vw	N1–N2–N3 asym stretch
1115	1111vw	N1–C–N4 sym stretch out of phase with N2–N3 stretch
1080	1070w	N1–C–N4 out-of-plane distortion, asym ring breathing
1027	1028w	N1–C–N4 and N–N(O)O symmetric stretch
1014	1011m	N2–N3 stretch
894	862w	C–N–NO_2 bending
770	763w	C out-of-plane distortion
740	738vw	Ring twist

[a] vs = 90−100%, s = 70−90%, m = 40−70%, w = 10−40%, vw <10%.

the predominately N–NO_2 stretching motion increases in energy (i.e. the bond shortens) as the negative charge increases [1226 cm^{-1} (I), 1315–cm^{-1} (II), 1398–cm^{-1} (III)]. Conversely, the –NO_2 asymmetric stretching energy decreases with the increase in the negative charge and the N–O bond distance [1613 cm^{-1} (I), 1423 cm^{-1} (II), 1295 cm^{-1} (III)].

In summary, salts of nitraminotetrazole are worthy of further consideration in the energetic materials field. In particular, the high thermal stability of the salts of (III) might make them useful as high-temperature-stable primary explosives. The thermal decomposition characteristics of these compounds will be presented [13] in a subsequent Special Issue of this journal dedicated to Andrew Galway and Mike Brown.

Acknowledgements

We are grateful to the Office of Naval Research for support of this work on N00014-95-1-1338.

References

[1] T.K. Highsmith, G.K. Lund, R.J. Blau, J.C. Hinshaw, D.W. Doll, US Patent 5,516,377, 10 January 1994.
[2] L.R. Bates, in: Proceedings of the 13th Symposium on Explosive Pyrotechnic, 1986, p. 2.

[3] E. Lieber, D.R. Levering, L.J. Patterson, Anal. Chem. 23 (1951) 1594.
[4] A.G. Mayants, V.S. Klimenko, V.V. Erina, K.G. Pyreseva, S.S. Gordeichuk, V.N. Leibzon, U.N. Burtev, Khim. Geterotsikl. Soedin. 8 (1991) 1067.
[5] A.G. Mayants, K.G. Pyreseva, S.S. Gordeichuk, Russia J. Org. Chem. 24 (1988) 798.
[6] A.G. Mayants, V.V. Erina, S.S. Gordeichuk, Russia J. Org. Chem. 25 (1989) 376.
[7] M.A. Ilyushin, A.N. Terpigorev, I.V. Tselinskii, Russia J. Gen. Chem. 10 (1999) 1654.
[8] A. Gao, A.L. Rheingold, T.B. Brill, Prop. Explos. Pyrotech. 16 (1991) 97.
[9] E. Lieber, E. Sherman, R.A. Henry, J. Cohen, J. Am. Chem. Soc. 73 (1951) 2321.
[10] M.J. Frisch, G.W. Trucks, H.B. Schlegel, G.E. Scuseria, M.A. Robb, J.R. Cheeseman, V.G. Zakrzewski, J.A. Montgomery Jr., R.E. Stratmann, J.C. Burant, S. Dapprich, J.M. Millam, A.D. Daniels, K.N. Kudin, M.C. Strain, O. Farkas, J. Tomasi, V. Barone, M. Cossi, R. Cammi, B. Mennucci, C. Pomelli, C. Adamo, S. Clifford, J. Ochterski, G.A. Petersson, P.Y. Ayala, Q. Cui, K. Morokuma, D.K. Malick, A.D. Rabuck, K. Raghavachari, J.B. Foresman, J. Cioslowski, J.V. Ortiz, B.B. Stefanov, G. Liu, A. Liashenko, P. Piskorz, I. Komaromi, R. Gomperts, R.L. Martin, D.J. Fox, T. Keith, M.A. Al-Laham, C.Y. Peng, A. Nanayakkara, C. Gonzalez, M. Challacombe, P.M.W. Gill, B. Johnson, W. Chen, M.W. Wong, J.L. Andrers, C. Gonzalez, M. Head-Gordon, E.S. Replogle, J. A. Pople, Gaussian Inc., Pittsburgh PA, 1998.
[11] G. Schaftenaar, J.H. Noordik, J. Comput. Aided Mol. Design 14 (2000) 123.
[12] L. Jaeger, C. Tretner, H. Hartung, M. Beidermann, C. Wagner, Z. Anorg. Allg. Chem. 629 (1998) 1558.
[13] B.C. Tappan, T.B. Brill, Thermochim. Acta, in Press.